Effect of process parameters on parts quality and process efficiency of fused deposition modeling

Maurizio Galetto [*], Elisa Verna, Gianfranco Genta

Department of Management and Production Engineering, Politecnico di Torino, Corso Duca degli Abruzzi 24, 10129 Torino, Italy

A R T I C L E   I N F O

A B S T R A C T

Fused Deposition Modeling (FDM) is an additive manufacturing technique for fabricating parts directly from computer-aided design data by melting, extruding, and resolidifying a thermoplastic filament. This paper presents a methodology for optimizing both process efficiency, i.e., time and energy consumption, and part quality, i.e., surface roughness and dimensional accuracy, of Polylactic Acid (PLA) components produced by FDM. In this work, a Design of Experiments (DoE) approach is adopted to quantify the effects of deposition parameters on process efficiency and part quality outputs. Specifically, the investigated input parameters are layer height, fill density, extruder temperature, part orientation, number of shells, print speed and retraction speed. The mathematical models relating the significant process parameters to the output responses are developed and the responses are optimized considering different scenarios. An experimental validation is performed to test the adequacy of such optimizations. These experimental results showed that, according to the context, different parameter settings pursue different goals in terms of part quality and process efficiency. The proposed approach may effectively help designers determine process parameters' settings to optimize both part quality and process efficiency and can be applied to either prototype or part production.

1. Introduction

Additive Manufacturing (AM) is worldwide recognized as "the process of joining materials to make parts from 3D model data, usually layer upon layer, as opposed to subtractive manufacturing technologies and formative manufacturing methodologies". Additive technologies have experienced significant growth over the past 30 years in terms of the number of machines sold and parts produced. By researchers and practitioners, AM is considered one of the most dynamic and promising recent industrial innovations (Nyaluke, An, Leep, & Parsaei, 1995; Wohlers, 2018). AM processes offer a novel approach for prototyping and manufacturing parts compared to traditional casting and metal-cutting processes. These technologies integrate computer-aided design (CAD) for creating a computer model of the final part with its manufacturing by adding layers of materials with dedicated equipment. Accordingly, it is possible to create spatially sophisticated and light-weight lattice components that would be impossible to obtain with traditional manufacturing techniques (Verna, Genta, Galetto, & Franceschini, 2020). The rapid growth and improvements in AM technologies have enabled many industrial sectors to reap the advantages

(Chergui, Hadj-Hamou, & Vignat, 2018; Lan & Ding, 2007). Typically, AM applications are found in the aerospace, energy, automotive, medical and dental, tooling and jewelry industries (Amini & Chang, 2018; Galetto, Genta, Maculotti, & Verna, 2020; Gardan, 2016; Majeed et al., 2020; Verna, Genta, Galetto, & Franceschini, 2019). One of the main solid freeform fabrication (SFF) processes recognized as an AM technology is Fused Deposition Modeling (FDM). This process is one of the most widely used, particularly for non-commercial use, due to its versatility in producing functional parts with complex geometry in reasonable production time (Rayegani & Onwubolu, 2014). In the FDM process, a thermoplastic filament is melted and extruded through a circular nozzle. The molten plastic is deposited onto a print bed through a nozzle movement, controlled through a 3-axis system. Thermoplastics are the most widely used feedstock materials, although different materials, including cement and composites, are also compatible with the FDM process (Abid et al., 2018; Li, Wang, Sun, & Yu, 2018; Liu et al., 2019; Stoof & Pickering, 2018). Due to the versatility of materials and shapes, FDM's main advantage is to produce polymeric complex-shaped components in one step. The major applications are functional prototypes for commercial and non-commercial use, rapid tooling patterns,

---

and concept models. Despite FDM benefits, many technical challenges continue to hamper widespread adoption and achieve its full potential. One major barrier is the variation in the part quality and mechanical properties, due to inadequate dimensional tolerance, presence of defects, surface roughness, and residual stress, which is not sufficient yet to meet the industrial sectors' stringent requirements (Dong, Wijaya, Tang, & Zhao, 2018; Perez, 2002; Wu, Wei, & Terpenny, 2018). Achieving high levels of surface roughness and dimensional accuracy of FDM parts is an extremely challenging task due to many factors, such as the high complexity of the underlying physical phenomena and transformations that take place during part production. Nowadays, there is no unique standard method to model and improve the surface quality and dimensional accuracy due to the complex nature of the process and the different properties of the material used. Indeed, several approaches have been adopted in the literature to this purpose, such as Design of Experiments (DoE), simulations and optimizations, involving different process parameters and their interactions. In particular, several attempts have been made to model the surface roughness of FDM parts. Ahn, Kweon, Kwon, Song, and Lee (2009) proposed a theoretical model to express surface roughness distribution according to changes in surface angle by considering the main factors that crucially affect surface quality. In the study of Anitha, Arunachalam, and Radhakrishnan (2001), parameters' influence on prototype quality characteristics using Taguchi technique was assessed. Pandey, Reddy, and Dhande (2003) described a methodology and software implementation that provide the designer with a computer graphics-based visualization of surface roughness. In the study of Durgun and Ertan (2014), the effect of five different raster angles for three orientations was tested on surface roughness, tensile strength, and flexural strength (Durgun & Ertan, 2014). Furthermore, several studies have been published in the literature on modeling the dimensional accuracy of FDM parts. Sood, Ohdar, and Mahapatra (2009) investigated the effect of different process parameters, such as layer height, part orientation, raster angle, air gap and raster width, on the dimensional accuracy of FDM processed ABSP400 (acrylonitrile-butadiene-styrene) parts. Also in the paper of Nancharaiah, Raju, and Raju (2010), the effect of layer height, road width, raster angle and air gap on the surface finish and dimensional accuracy was investigated. Sahu, Mahapatra, and Sood (2013) presented experimental data and a fuzzy decision-making logic combined with Taguchi method for improving the dimensional accuracy of FDM processed ABSP 400 parts. Garg, Bhattacharya, and Batish (2016) investigated the effect of part deposition orientation on surface finish and dimensional accuracy of FDM parts. Previous research has also investigated the effect of several process parameters on the FDM process's efficiency in terms of printing time and energy consumption (Frank, Chandra, & Schmitt, 2015; Griffiths, Howarth, Rowbotham, & de-A., & Rees, A. , 2016). It is evident from the literature that several input parameters can be controlled and varied in order to optimize the selected output parameters, involving efficiency and quality of FDM parts (Pandey, Thrimurthulu, & Reddy, 2004). In this work, a methodology for choosing the input parameters is proposed and implemented. When a combination of different input variables and their interactions affect selected responses, the Design of Experiments (DoE) is an effective statistical approach for optimizing the process (Mason, Gunst, & Hess, 2003; Verna, Biagi, et al., 2020).

This paper aims at investigating FDM processed PLA (Polylactic Acid) parts through statistically designed experiments to determine the significance of the process parameters affecting parts quality (surface roughness and dimensional accuracy) and process efficiency (printing time and energy consumption). To date, few detailed studies have proposed a combined analysis of the quality and efficiency of parts produced by the FDM process. This investigation attempts to provide a reference procedure to determine the combination of process parameters that optimize both part quality and process efficiency, with the minimum number of tests. To this end, a fractional factorial design is performed. The Analysis Of Variance (ANOVA) is used to estimate the statistical significance of parameters' effects on the observed differences
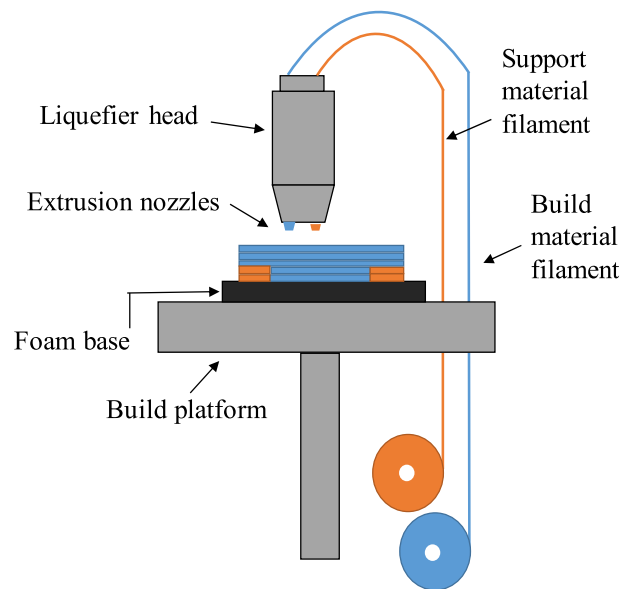

Fig. 1. Schematic of the FDM process.

in the selected responses. The adequacy of the obtained models is demonstrated by using the coefficients of determination, and the residual plots are analyzed to verify the basic assumptions to perform the ANOVA. The mathematical models relating the significant process parameters to the output responses are derived and optimized, considering different scenarios. Finally, new samples are produced to test the models' adequacy and the optimizations performed in each scenario. The findings should make an important contribution to the field of FDM production by supporting designers in the improvement of process efficiency and parts quality, according to their objectives.

It is worth remarking that, in the scientific literature, it has been shown that some parameters may have a quadratic effect on responses (Lužanin, Movrin, & Plančak, 2014; Sanatgar, Campagne, & Nierstrasz, 2017). To this end, four central points are added to the experiment, which allowed evaluating the model's curvature. However, since the effects of each quadratic term of the model cannot be estimated without performing further tests, i.e., by adding axial points, these models may not be used for forecasting purposes (Myers & Montgomery, 1995). Further tests will aim at estimating the quadratic effects, thus improving the predictions and optimizations obtained in this paper. Despite this limitation, the proposed methodology can represent an effective and efficient approach to support researchers and practitioners.

The remainder of this paper is organized into five sections, including one appendix. Section 2 presents the FDM process and the produced PLA samples. Section 3 contains the description of the design of experiments and the related experimental details. Section 4 contains the performed analysis with the related experimental results and discussion. Section 5 summarizes the results obtained, specifying the practical implications and insights for future research. The Appendix section provides further information to support the proposed analysis.

2. FDM process and samples

2.1. FDM machine

The AM machine used in this study is the MakerBot z18. It is characterized by a layer resolution of 100 μm and an on-board camera to remotely monitor the print progress. Besides, it enables the production of both prototypes and finished products due to the high performance, including high speed, good reliability and free design, in a build volume of 30.0 L × 30.5 W × 45.7H cm. Shortly, in the machine MakerBot z18, the filament is fed into the extruder of the printer, where it is heated to a

Table 1
Qualitative matrix of relation between process parameters and responses, according to literature and experts' evaluations.

Category	Parameter	Printing time [min]		Energy consumption [kWh]		Surface roughness [μm]		Dimensional accuracy [mm]	
		Literature	Expert	Literature	Expert	Literature	Expert	Literature	Expert
(i)	Print Speed [mm/s]	4	4	4	4	3	3	4	4
(i)	Layer Height [mm]	5	5	4	4	5	5	4	4
(i)	Fill Density [%]	5	4	4	4	2	1	4	3
(i)	Extruder temperature [°C]	NC	NC	4	4	2	2	3	3
(i)	Number of shells [–]	4	4	3	3	3	1	3	2
(i)	Bottom/Top thickness [mm]	3	2	2	2	2	1	2	2
(i)	Retraction speed [mm/s]	4	1	2	1	3	NC	3	NC
(i)	Retraction distance [mm]	3	1	2	1	3	NC	3	NC
(ii)	Filament diameter [mm]	1	NC	1	NC	3	2	2	2
(iii)	Part orientation [°]	1	NC	2	NC	4	4	4	4

temperature high enough to melt it. Then, it is extruded from a nozzle to create an object, each layer at a time. The machine is provided with a nozzle with a diameter of 0.4 mm. Furthermore, it does not have a heated build plate, and thus it operates at room temperature (between 15 °C and 24 °C). A schematic representation of the FDM machine is provided in Fig. 1.

2.2. Process parameters

A considerable amount of literature focused on the effect of FDM process parameters on parts quality and process efficiency. These process parameters can be grouped into three categories (see also Table 1):

(i) Process-specific influencing variables: layer height, bed temperature, nozzle temperature, fill density, print speed, infill speed, retraction distance, retraction speed, initial layer height, initial layer line width, bottom layer speed, raster angle, raster width, air gap, number of shells, shell thickness, bottom/top thickness, outer shell speed, inner shell speed;

(ii) Machine-specific influencing variables: nozzle diameter, speed of material feeding rollers, filament width, layer height, platform adhesion type, temperature of removal, filament diameter;

(iii) Geometries-specific influencing variables: part orientation, particular features.

The parameters listed above are first reduced by selecting the parameters that are actually controllable on the MakerBot z18. For instance, parameters such as nozzle diameter or bed temperature are not considered in the present analysis because they cannot be modified and controlled in the adopted AM machine. Secondly, a qualitative matrix of relation is created to identify not significant parameters (see Table 1). In the column "Literature", the evaluations are related to the relations identified in the literature. A nominal scale from 1 to 5 is adopted. This 5-point scale is chosen because it enables the evaluator to clearly distinguish between the various levels, without generating ambiguity and/or item omissions in the evaluation process (Agresti, 2003; Franceschini et al., 2007, 2019). Specifically:

- 5 is assigned when three or more papers identified a relation between the process parameter and the response;
- 4 means that two papers showed the existence of a relation among the variables;
- 3 is assigned when one paper proved a relation among the variables;
- 2 when one paper suggested that no relation exists;
- 1 when more than one paper showed the non-relation between the parameter and the response;
- NC, i.e., not classifiable, is introduced when no paper investigated the relation between the parameter and the response.

The matrix reported in Table 1 also includes the evaluation of experts in the FDM process. Three experts were interviewed since three can be

considered the minimum acceptable number for obtaining reliable evaluations without significantly increasing the cost of acquiring information (Franceschini, Galetto, & Maisano, 2019). The experts' evaluation, obtained according to the 5-points scale, is reported in the column "Expert". Finally, process parameters having at least one evaluation equal to 4 in the relation matrix are chosen as potential control factors for the planned experimentation. These parameters are: print speed, layer height, fill density, extruder temperature, part orientation, number of shells, retraction speed. Although part orientation was significant, it is not considered in this study as the aim is to produce parts without using supports. To this purpose, new experiments will be designed to evaluate part orientation's effect on selected responses. It has to be remarked that the selection of process parameters for the DoE, also called pre-experimental planning, requires in-depth process knowledge. According to Montgomery (2017), different techniques can support designers in this phase, such as cause-and-effect diagrams. However, no standard procedure exists. In this paper, rather than relying only on prior knowledge, a structured method has been proposed that combines literature review and practical experience.

Finally, the six process parameters considered are described in detail.

1. Print speed: this parameter specifies the printing speed used during the process. It influences the speed of material deposition. Frank et al. (2015) included print speed as one of the seven input parameters for the experiment and discovered that this factor has a statistical influence on the overall time needed to finish a printed part.

2. Layer height: layer height represents the thickness of each printed layer. It is equivalent to vertical resolution in FDM parts. The thinner the layer, the smoother the printed object's texture, but more time is required. This strictly depends upon the type of nozzle used (Anoop K Sood, Ohdar, & Mahapatra, 2012). The standard nozzle diameter on MakerBot z18 is 0.4 mm, and therefore, this is the highest layer height that can be achieved. In literature, several studies have investigated the key role of layer height in FDM processes (Anitha et al., 2001; Frank et al., 2015; Griffiths et al., 2016; Onwubolu & Rayegani, 2014; Pandey et al., 2003; Pennington, Hoekstra, & Newcomer, 2005; Sood et al., 2012).

3. Fill density: the infill percentage gives the support structure inside the object and can be varied depending on the part's application field. The density of the part is strictly related to the infill percentage. A higher percentage will result in a more robust object, while 0% infill will make the object hollow. When a prototype is only used for shape and fit testing, the infill percentage can be decreased, allowing it to be made at a lower cost and faster. Griffiths et al. (2016) included fill density and other three process parameters to investigate the relation among these and output variables.

4. Extruder temperature: this is the temperature of the nozzle. This parameter affects the viscosity of the polymer. In the research of Frank et al. (2015), it was shown that the high temperature of the nozzle strongly impacts the shrinkage. Kaveh, Badrossamay, Foroozmehr, and Etefagh (2015) investigated the effect of the extruder
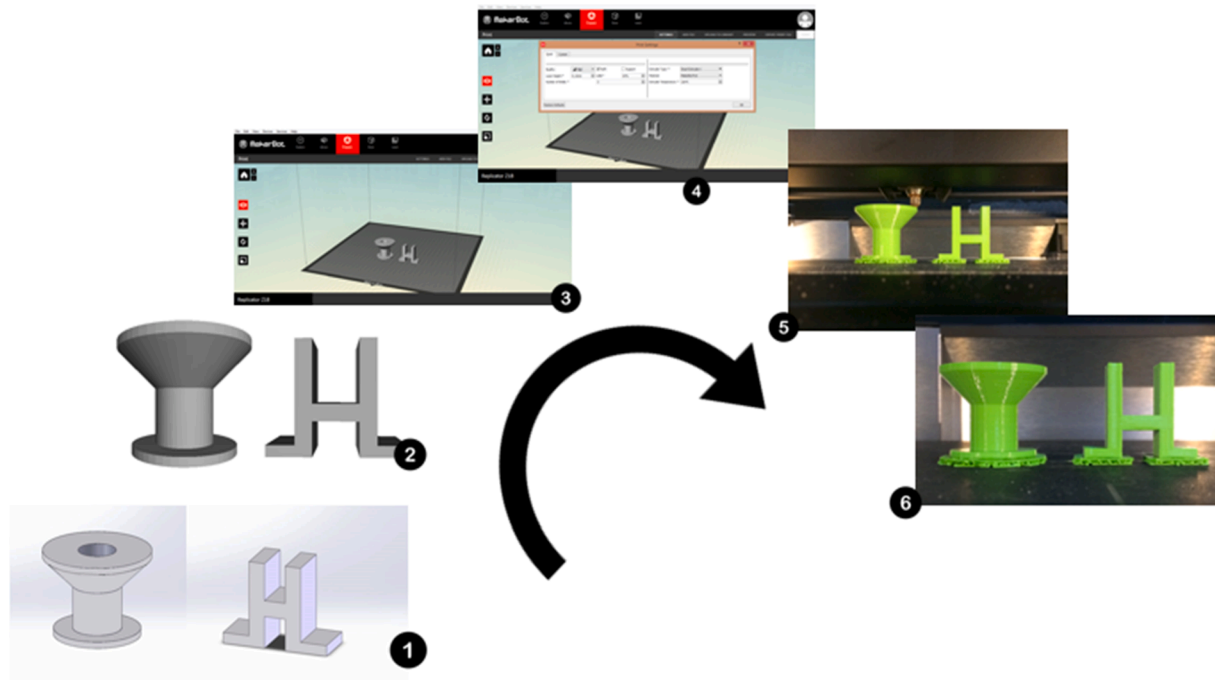
Fig. 2. The six steps to produce the samples (3D model creation, STL file, File transfer to the machine, Machine setup, Build, Part removal).
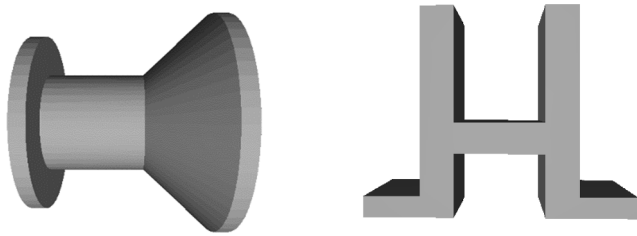

Fig. 3. Prototypes of a connector for a pump and of a door's hinge.

temperature on precision and internal cavity of geometries produced by FDM. The results showed that the temperature affects both the output variables (Kaveh et al., 2015).

5. Number of shells: a shell is a border that is extruded for each layer. The minimum number of shells per layer is one (Griffiths et al., 2016). Adding more shells does not affect its external dimensions but can make the part stronger. The number of shells is one of the process parameters considered by Griffiths et al. (2016) in their research.

6. Retraction speed: the retraction speed gives information on how fast the filament is retracted. In many cases, this parameter is not considered in investigations. However, since two parts are printed together in this study, the retraction speed might significantly affect part final quality and printing time.

2.3. PLA samples

Two FDM processed PLA (polylactic acid) samples are produced, following the six steps illustrated in Fig. 2: 3D model creation, STL file, File transfer to the machine, Machine setup, Build, Part removal (Gibson, Rosen, & Stucker, 2014).

Two shapes considered "problematic features" in literature are designed to analyze how the machine works under stressed conditions. The two samples that are produced together in the same job are an overhang and a bridge. They can be seen, respectively, as prototypes of a connector for a pump and a door hinge (see Fig. 3).

Regarding the prototype of a connector for a pump, the main features

Table 2
Levels of process parameters.

Process parameter	Symbol	Minimum value	Center value	Maximum value
Layer height	L [mm]	0.12	0.20	0.31
Fill density	F [%]	5	10	20
Extruder Temperature	T [°C]	205	215	220
Number of shells	S [–]	1	2	3
Print speed	P [mm/ s]	140	150	160
Retraction speed	R [mm/ s]	45	50	60

are the overhanging surfaces. An overhang occurs when the material on the printed layer is partially supported by the underlying layer. At 45°, the newly printed layer is supported by 50% of the previous layer, allowing sufficient support and adhesion to build on it. Above 45°, although overhanging features may be produced without supports, the angled surface begins to suffer in quality due to the molten filament's inherent stickiness (Montero, Roundy, Odell, Ahn, & Wright, 2001). For that reason, supports are highly recommended. Another issue that occurs when printing overhangs is curling. The newly printed layer becomes increasingly thinner at the overhang's edge, resulting in differential cooling causing it to deform upward (Gibson et al., 2014). For these two reasons, the prototype in Fig. 3 is designed with an overhang of 45° to stress this boundary condition.

Concerning the second prototype, the door's hinge, it is characterized by a bridge structure. Bridging occurs when the machine has to deposit material between two supports or anchor points. In general, the shorter is the length of the bridge, the greater is its structural success. Instead, the longer the bridge, the more post-processing and supports will require (Gibson et al., 2014). The bridge is 24 mm in length in the sample produced and is printed without supports.

Table 3
Arrangement of the two-level factorial with half fractional design for the six process parameters used in the present study.

Run Order	L [mm]	F [%]	T [°C]	S [–]	P [mm/s]	R [mm/s]
1	0.310	0.050	205	3	140	45
2	0.120	0.200	220	1	160	60
3	0.310	0.200	205	1	140	45
4	0.310	0.200	220	1	140	60
5	0.310	0.200	220	3	140	45
6	0.310	0.200	205	1	160	60
7	0.310	0.200	220	3	160	60
8	0.310	0.050	220	1	160	60
9	0.310	0.050	205	3	160	60
10	0.310	0.200	220	1	160	45
11	0.310	0.200	220	3	140	60
12	0.120	0.050	205	3	140	60
13	0.310	0.050	205	1	160	45
14	0.120	0.200	205	3	140	45
15	0.120	0.050	205	3	160	45
16	0.120	0.200	220	3	140	60
17	0.120	0.050	220	1	140	60
18	0.120	0.050	205	1	140	45
19	0.120	0.200	205	1	160	45
20	0.120	0.050	220	1	160	45
21	0.120	0.200	220	1	140	45
22	0.120	0.200	205	3	160	60
23	0.120	0.050	205	1	160	60
24	0.310	0.200	205	3	140	60
25	0.310	0.050	220	1	140	45
26	0.120	0.200	205	1	140	60
27	0.120	0.050	220	3	140	45
28	0.120	0.050	220	3	160	60
29	0.310	0.050	220	3	160	45
30	0.310	0.200	205	3	160	45
31	0.310	0.050	205	1	140	60
32	0.120	0.200	220	3	160	45

Fig. 4. Measurements of the surface roughness. Surface 1 and Surface 2 are analyzed on the overhang, while Surface 3, Surface 4 and Surface 5 on the bridge.

models correlating each response with the relevant parameters.

3. Design of experiments and experimental details

3.1. Design of experiments

As abovementioned, the six process parameters or control factors chosen are: layer height (L), fill density (F), extruder temperature (T), number of shells (S), print speed (P), and retraction speed (R). These parameters were kept at two levels, i.e., "minimum value" and "maximum value" (Table 2). Minimum, center and maximum values of each process parameter were obtained starting from the default values suggested by the producer, also taking into account the values used in the scientific literature and the empirical tests carried out on the machine in preliminary tests. From the manufacturing viewpoint, the levels of each process parameter can be set in the FDM machine through the MakerBot Desktop application before each planned test.

With respect to the traditional full-factorial experimental plan, which would require 64 tests, a two-level factorial with half fractional design is performed, resulting in 32 experiments (see Table 3). The order of the tests is randomized. This half fractional design with six control factors is a Resolution VI design. This means that no main effects or 2-factor interactions are aliased with any other main effects or 2-factor interactions. However, 2-factor interactions are aliased with 4-factor interactions and main effects are aliased with 5-factor interactions (Montgomery, 2017). The complete list of the aliases generated by the half factorial design is provided: $L = F \cdot T \cdot S \cdot P \cdot R$, $F = L \cdot T \cdot S \cdot P \cdot R$, $T = L \cdot F \cdot S \cdot P \cdot R$, $S = L \cdot F \cdot T \cdot P \cdot R$, $P = L \cdot F \cdot T \cdot S \cdot R$, $R = L \cdot F \cdot T \cdot S \cdot P$, $L \cdot F = T \cdot S \cdot P \cdot R$, $L \cdot T = F \cdot S \cdot P \cdot R$, $L \cdot S = F \cdot T \cdot P \cdot R$, $L \cdot P = F \cdot T \cdot S \cdot R$, $L \cdot R = F \cdot T \cdot S \cdot P$, $F \cdot T = L \cdot S \cdot P \cdot R$, $F \cdot S$ $L \cdot T \cdot P \cdot R$, $F \cdot P = L \cdot T \cdot S \cdot R$, $F \cdot R = L \cdot T \cdot S \cdot P$, $T \cdot S = L \cdot F \cdot P \cdot R$, $T \cdot P = L \cdot F \cdot S \cdot R$, $T \cdot R = L \cdot F \cdot S \cdot P$, $S \cdot P = L \cdot F \cdot T \cdot R$, $S \cdot R = L \cdot F \cdot T \cdot P$, $P \cdot R = L \cdot F \cdot T \cdot S$.

The ANOVA is applied to assess if the observed differences in the responses, caused by the parameters' variation, are systematic rather than physiological. Therefore, the statistically significant parameters identified using the ANOVA are used as predictors in the regression
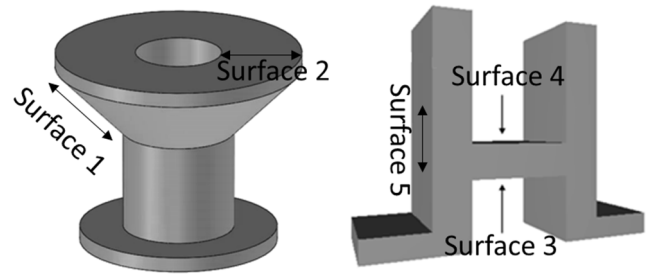
3.2. Experimental details

Following the experimental plan, the 32 printing jobs resulted in 64 parts: 32 parts representing the connector for the pump and 32 parts representing the door's hinge. After the production, measurements are performed. The Printing Time (*PT*) and the Energy Consumption (*EC*) data are measured during the printing process for each job. Data for each job's energy consumption have been collected during the process using the Energy Logger 4000 EKM device by VOLTCRAFT. It is worth remarking that printing time and energy consumption values are not representative of a single object. Indeed, they are relevant to each job, which consists of the two parts together.

For the surface roughness and the dimensional accuracy, the parts are marked and measured afterward. In detail, the surface roughness is measured according to industrial standards ISO 4287 and ISO 4288, using a roughness tester RTP80 with a 2 μm radius stylus tip (ISO 4287:2009; ISO 4288:2000). Two surfaces for the overhang (Surface 1 and Surface 2) and three for the bridge (Surface 3, Surface 4 and Surface 5) are measured (see Fig. 4). For such surfaces, characterized by a periodic profile due to the process's intrinsic characteristics, the prescribed sampling length is based on the mean width of profile elements (*RSm*). When *RSm* is included between 0.4 mm and 1.3 mm, it is recommended to use a sampling length for filtering (cut-off length) of 2.5 mm and an evaluation length of 12.5 mm [38]. The Robust Regression Gaussian Filter, defined in ISO 16610–31, is used (ISO 16610-31:2016). It is an iterative algorithm that calculates local weights based on the distance between the primary and waviness profiles. This filter is the preferred choice for structured surfaces, stratified surfaces and in the presence of form, grooves or pores (ISO 16610-31:2016). In addition to the parameter *RSm*, the roughness parameter calculated from the filtered roughness profile is *Ra*, defined as the average value of the ordinates from the centerline. It is theoretically derived as the arithmetic average value of departure of the profile from the mean line along a sampling length. Three measurements, each spaced as far apart as possible on the surface, in the direction perpendicular to the deposition path, are performed on each surface of the samples. The *Ra* and *RSm* values are derived and the average values are examined. Accordingly, each surface, both of the overhang and the bridge, is characterized by two output variables (for instance, Surface 1 by *Ra1* [μm] and *RSm1* [mm]).

These measurements aim to evaluate the effect of the different orientations of the surfaces with respect to the build direction on the parts surface quality. Since the two different geometries are built in the orientation of Fig. 4, it is expected that Surface 3 and Surface 1 are rougher than Surface 2 and Surface 4. This expectation will be confirmed by analyzing the *Ra* and *RSm* values (see next Section 4). An example of the graph obtained by the surface roughness tester is provided in Fig. 5.

For dimensional accuracy, the parts are measured using a digital caliper with a resolution of one-hundredth of a millimeter. One measure for each dimension is taken afterward (see Fig. 6). Since the parts are
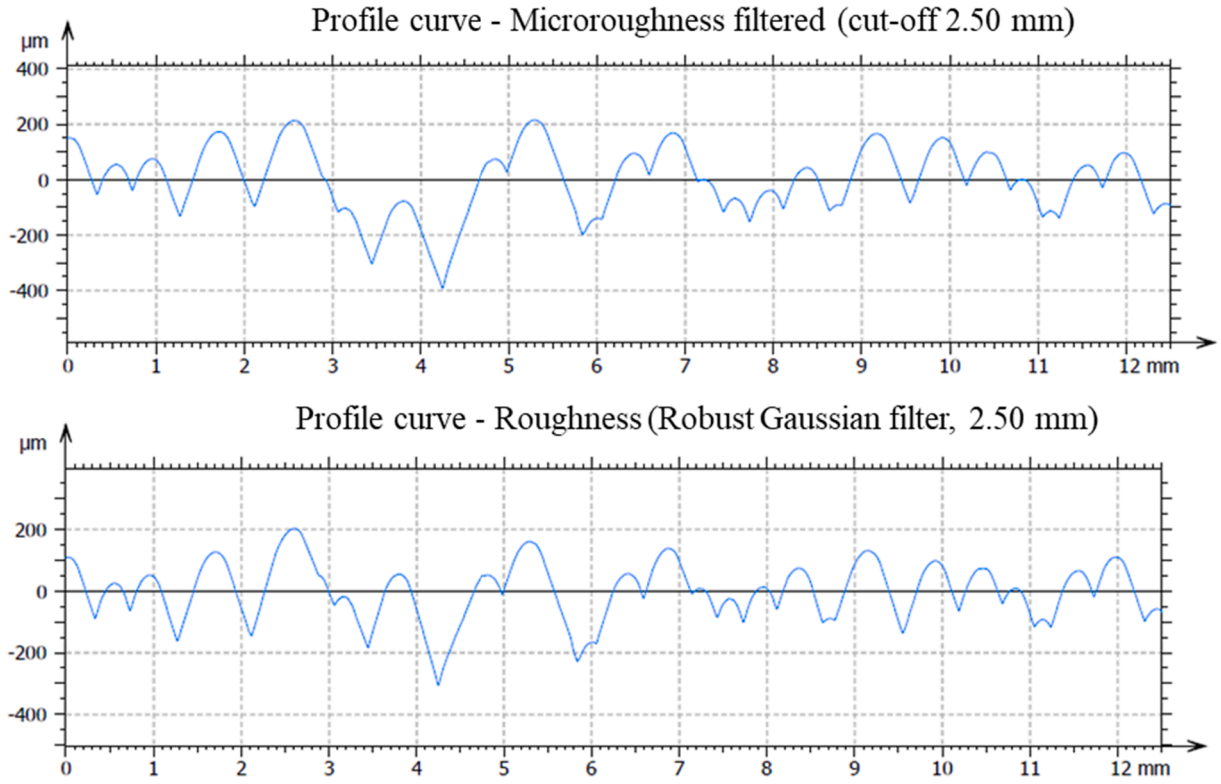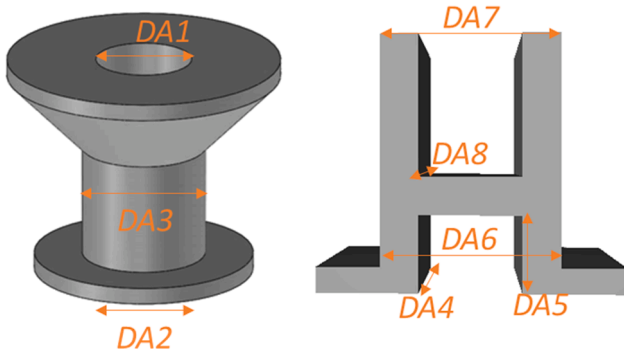
Fig. 5. Surface Roughness Graph of Surface 1.

Fig. 6. Measurements of dimensional accuracy.

created as prototypes, the dimensions measured are the ones that may require a more stringent tolerance, rather than the total height, width, and length, which could vary within certain limits. The target values of the dimensions that need to be achieved by the two prototypes are as follows: $DA1 = DA2 = 14.59$ mm, $DA3 = 18.76$ mm, $DA4 = DA8 = 13.34$ mm, $DA5 = 10.00$ mm, $DA6 = DA7 = 23.35$ mm, $DA8 = 13.65$ mm. The measurement results for all the responses are reported in Table A.1.

4. Experimental results and discussion

4.1. DoE analysis

The experiment aims to optimize the process parameters in the FDM process to get better responses. In detail, the objectives are minimizing printing time, energy consumption and surface roughness, and maximizing dimensional accuracy (i.e., minimizing the deviation from the target value of each dimension). The arrangement of the DoE allows the development of the appropriate empirical equations (first-order multiple linear regression equations, including two-way interactions), defined as follows:

$$y_j = \beta_0 + \beta_1 x_1 + \beta_2 x_2 + \beta_3 x_3 + \beta_4 x_4 + \beta_5 x_5 + \beta_6 x_6 + \beta_{12} x_1 x_2 + \beta_{13} x_1 x_3 + \\ + \beta_{14} x_1 x_4 + \beta_{15} x_1 x_5 + \beta_{16} x_1 x_6 + \beta_{23} x_2 x_3 + \beta_{24} x_2 x_4 + \beta_{25} x_2 x_5 + \beta_{26} x_2 x_6 + \\ + \beta_{34} x_3 x_4 + \beta_{35} x_3 x_5 + \beta_{36} x_3 x_6 + \beta_{45} x_4 x_5 + \beta_{46} x_4 x_6 + \beta_{56} x_5 x_6$$

(1)

where y_j ($j = 1, \ldots, 20$) corresponds to each response of Table A.1 (*PT, EC, DA1-DA8, Ra1-Ra5, RSm1-RSm5*).

The predicted response (y_j) is therefore related to the set of regression coefficients (β): the intercept (β_0), linear ($\beta_1, \beta_2, \beta_3, \beta_4, \beta_5, \beta_6$), and interaction ($\beta_{12}, \beta_{13}, \beta_{14}, \beta_{15}, \beta_{16}, \beta_{23}, \beta_{24}, \beta_{25}, \beta_{26}, \beta_{34}, \beta_{35}, \beta_{36}, \beta_{45}, \beta_{46}, \beta_{56}$). The software MINITAB® is used to perform the analysis. The ANOVA, the coefficients for each factor and their *p*-values (see Table A.2) are obtained separately for each response.

In order to reveal the cause-and-effect relationships between the six factors and the twenty responses, a first qualitative analysis for each response may be carried out through the analysis of the "Interaction plot". This plot is used to visualize possible interactions between variables. If there is no interaction, the lines in the plot are parallel. On the contrary, the higher the degree of interaction, the greater is the difference in slope between the lines. However, the interaction plot does not tell if the interaction is statistically significant. For *DA1* (see Fig. 7), many interactions between parameters appear to be evident, such as the interactions between *L* and *F*, *L* and *T*, *F* and *T*, *L* and *P*, *S* and *P*, *F* and *S*.

Through the ANOVA, the significance of every single main effect and interactions between variables is derived separately for each response. Furthermore, the coefficients of determination (R-Sq [%], R-Sq adj [%]) have been calculated for each variable. These values indicate whether the model fits the data adequately or not. The R-Sq value always increases when additional predictors are added to a model, whereas the R-Sq adj shows in percentage how much the model explains the variance of the responses considering the numbers of predictors (Myers & Montgomery, 1995). The R-Sq for the printing time is 99.99% and for energy
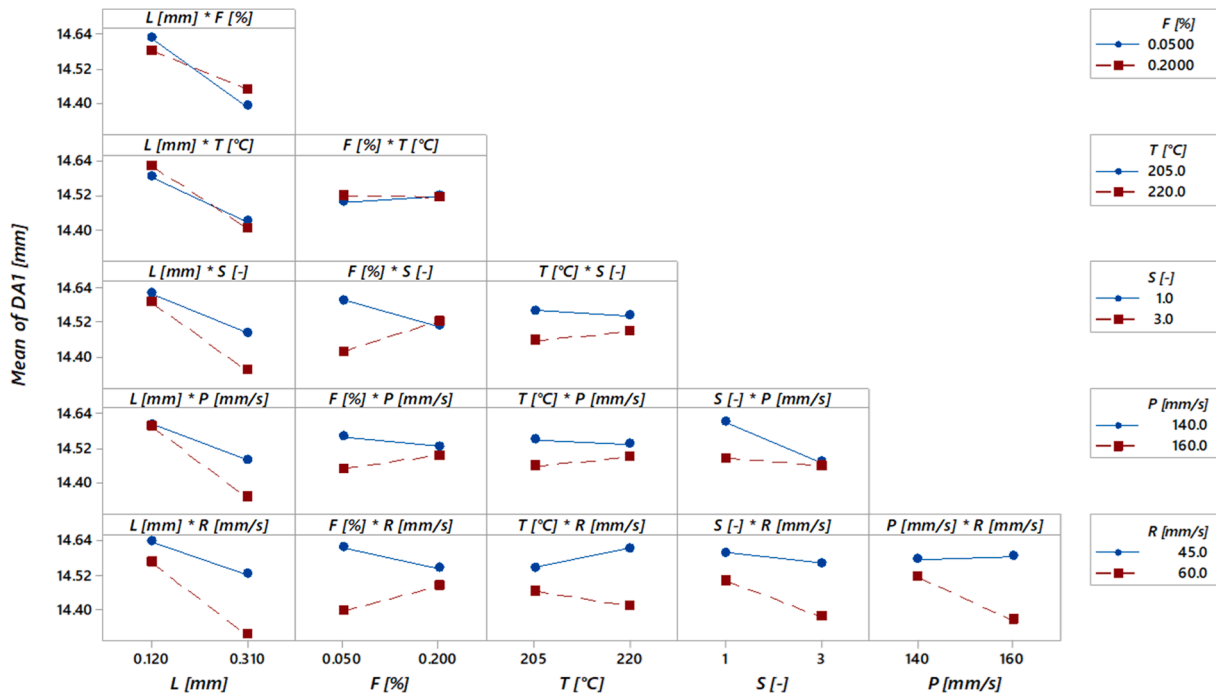
Fig. 7. Interaction plot for *DA1* [mm]

consumption is 99.92%. For the dimensional accuracy of the bridge, the R-Sq varies from 92.49% to 68.09%; for the overhang from 93.40% to 84.14%. Concerning the *Ra* surface roughness parameters, the co-efficients of determination for the overhang are 97.57% and 90.79%, and for the bridge varies from 77.83% and 92.07%. As far as *RSm* parameters are concerned, R-Sq related to the overhang are 97.53% and 75.85%, and for the bridge varies from 71.70% and 85.81%.

Based on the results, the models are subsequently reduced through the standard stepwise regression. This method both adds and removes predictors as needed for each step. It stops when all variables not in the model have *p*-values greater than the specified Alpha-to-Enter value and when all variables in the model have *p*-values less than or equal to the specified Alpha-to-Remove value (Montgomery, Runger, & Hubele, 2009). According to the literature, the Alpha-to-Enter and Alpha–to–Remove values are set to 0.15 (15%) (Wiegand, 2010). The new *p*-values obtained from ANOVA are reported in Table 4. In the table, differentiation among the factors which have *p*-value $\leq$ 1% (a very significant influence) and *p*-value $\leq$ 5% (a significant influence) is introduced. The factors with *p*-value $\leq$ 1% are double-asterisked and the factors with *p*-value $\leq$ 5% are asterisked. If a term is not included in the model after the stepwise procedure, then no *p*-value is reported in the table. Comparing the R-Sq adj of the reduced models with the previous ones, all the coefficients increased or remained constant, indicating that the terms deleted are not significant.

A mathematical model of the relationship between process parameters and each response is developed by regression analysis, based on the previous analysis. The complete list of regression models is given in Table A.3 and their measures of goodness-of-fit in Table 4. For example, the following mathematical model is developed for the response *DA1* [mm] (obtaining R-Sq = 68.33%):

$$DA1 = 11.02 + 1.56L - 0.0995S + 0.0249P + 0.0839R - 0.0482L \cdot R \\ + 0.471F \cdot S - 0.0152F \cdot R - 0.000542P \cdot R \tag{2}$$

Besides, the surface plots of each response are obtained. In Fig. 8, the surface plot of *DA1* versus *F* and *L*, and *DA1* versus *P* and *S* are reported.

As shown in Table A.3, depending on the model considered, process parameters and interactions can have a direct or inverse proportionality effect. For instance, considering dimensional accuracy responses (DA1-

DA8), layer height can have a directly proportional effect (as for DA1 and DA2) or an inversely proportional effect (as for DA3 and DA4). Therefore, given the complexity of the production process, identifying the different mathematical relationships between process parameters and responses is fundamental for improving the production process. In particular, as it will be described in the next Section 4.3, the modeling of the responses will enable to perform optimizations and thus obtain the optimal parameter sets.

Moreover, for every regression model, externally studentized residuals, also called studentized deleted residuals, are obtained (Montgomery, Peck, & Vining, 2012). The analysis of residuals is essential to understand if the ordinary least squares assumptions are satisfied. If these assumptions are fulfilled, then the regression produces unbiased coefficient estimates with the minimum variance (Montgomery et al., 2009). In detail, the following tests on externally studentized residuals are performed. Firstly, a normal Quantile-Quantile (Q-Q) plot of residuals for each selected regression is obtained. If the data points follow a 45° line, the normality assumption is likely to hold. Secondly, a test on the sample Skewness and Kurtosis (both approximately normal) of the residuals for each selected regression is carried out (Joanes & Gill, 1998). If both tests pass, the normality assumption is strengthened. Besides, a Shapiro-Wilk test on those same residuals for a final confirmation of normality is performed (Shapiro & Wilk, 1965). Finally, a Box and Whisker Plot for residuals is constructed to check for outliers (Devore, 2011). For instance, considering the regression model in Eq. (2) which refers to DA1, the normal Q-Q plot of residuals provided in Fig. 9 shows that residuals follow a normal distribution. The Skewness test and the Kurtosis test ($\alpha = 0.05$) cannot reject the null hypothesis of a normal distribution of residuals (*p*-value is, respectively, 0.97 and 0.70). Also, by performing the Shapiro-Wilk normality test ($\alpha = 0.05$), the null hypothesis of a normal distribution of residuals cannot be rejected (*p*-value = 0.71). From the Box and Whisker Plot, no outlier has been identified. The described procedure was applied to the externally studentized residuals of all the regression models reported in Table A.3. The normal Q-Q plots and the normality tests failed to reject the hypothesis of normality of residuals for all the models. However, some outliers have been identified by the Box and Whisker Plots. In detail, the residuals detected as outliers correspond to the following tests: test no. 2 for *EC*,

Table 4

p-value [%] table resulting from ANOVA after the stepwise regression (Alpha-to-Enter = Alpha-to-Remove = 15%).

	PT [min]	EC [kWh]	DA1 [mm]	DA2 [mm]	DA3 [mm]	DA4 [mm]	DA5 [mm]	DA6 [mm]	DA7 [mm]	DA8 [mm]	Ra1 [μm]	Ra2 [μm]	Ra3 [μm]	Ra4 [μm]	Ra5 [μm]	RSm1 [mm]	RSm2 [mm]	RSm3 [mm]	RSm4 [mm]	RSm5 [mm]
L [mm]	<0.1**	<0.1**	<0.1**	<0.1**	<0.1**	0.3**		<0.1**	<0.1**	11.2	<0.1**	<0.1**	<0.1**	<0.1**	0.3**	<0.1**	0.1**	<0.1**		7.3
F [%]	<0.1**	<0.1**		7.0	0.2**			0.6**	0.6**					0.2**			0.7**		3.7*	
T [°C]		<0.1**					1.7*	1.5*	0.9**			5.2	12.1		7.9					
S [-]		<0.1**	7.5	<0.1**	<0.1**	<0.1**					11.9					<0.1**				
P [mm/s]			12.2								<0.1**					10.6				
R [mm/s]			0.3**				5.5				9.6				11.3					
L·F [mm]				14.5		6.8	14.6												11.6	
L·T [mm·°C]		0.2**		0.5**		7.8	1.9**							0.1**	14.3					
L·S [mm]	<0.1**	<0.1**			<0.1**	<0.1**	12.6	1.1*			<0.1**	0.6**	7.2			<0.1**			3.8*	
L·P [mm²/s]				0.4**	6.9		0.6**	7.0	4.0*	12.4	9.3					6.1				
L·R [mm²/s]			12.8														0.3**			14.4
F·T [°C]		5.1	3.3*		1.3*	5.3	8.2		4.6*		3.7*		14.4		9.3*	3.9*			0.5**	
F·S [-]	<0.1**	0.1**		3.5*	0.1**	6.0							11.5		4.7*					12.0
F·P [mm/s]								2.6*			8.5							6.5		
F·R [mm/s]			7.5	5.7		10.0		2.0*	5.2	0.6**	14.6	9.1				7.8		3.7*		
T·S [°C]						10.0														
T·P [°C·mm/s]																				
T·R [°C·mm/s]				1.6*	0.3**	4.0*	0.2**	7.9	1.0**	5.7	6.2		3.8*	1.2*	0.2**	3.7*		2.6*		0.3**
S·P [mm/s]				<0.1**						13.1	13.9	9.1			4.1*	2.1	10.8		7.1	
S·R [mm/s]			7.5	3.5*								8.8					13.0		2.8*	
P·R [mm²/s²]																				
R-Sq [%]	99.97	99.88	68.33	88.86	90.60	80.74	66.67	81.18	77.90	44.07	95.53	86.39	90.25	74.31	65.26	95.44	60.72	80.46	58.48	41.54
R-Sq adj [%]	99.96	99.84	57.31	83.55	87.33	71.57	55.08	74.64	71.45	33.32	94.62	83.77	87.91	70.51	53.18	93.57	53.16	77.56	46.37	32.88

test no. 1 and 24 for *Ra1* and *RSm1*, test no. 22 for *Ra2*, test no. 26 for *Ra4*, and test no. 23 for *DA5*. The prevalence of outliers related to roughness measurements can be justified by the fact that in FDM parts, typically, the extent of roughness defects is greater than that of other issues, such as dimensional or process faults (Wickramasinghe, Do, & Tran, 2020). Additional normal Q-Q plots and normality tests results on externally studentized residuals are provided in Fig. A.1 for the responses *PT*, *EC*, *Ra5* and *RSm5*.

4.2. Evaluation of quadratic effects

In the scientific literature, it has been demonstrated that some parameters may have a quadratic effect on the responses (Lužanin et al., 2014; Sanatgar et al., 2017). To this end, four central points are added to the experiment, allowing the evaluation of the model's curvature. As shown in Table A.4, which reports the *p*-values resulting from the ANOVA of the stepwise regression procedure, the quadratic effect is significant for some responses, including *PT*, *EC*, *DA2*, *Ra1*, *Ra4* and *RSm1*. By introducing these 4 points, the R-Sq adj of most of the models has improved or remained unchanged. However, R-Sq adj has been reduced for *DA1*, *DA4*, *DA5*, *DA8*, *Ra1*, *Ra3*, *Ra4* and *RSm1*. Although some models present a curvature, it is impossible to attribute the quadratic effect to a specific process parameter. In fact, only one quadratic effect at a time can be estimated because of the used design: starting from a fractional design and adding center points, the vectors of quadratic terms are all the same. As a result, all quadratic effects are aliased among them. For that reason, without further experiments, no regression curves can be derived for forecasting and optimization. Future research will include replications and axial points (also called star points) to estimate all the quadratic effects and improve forecasting models accordingly.

4.3. Optimization

In order to optimize the responses, the regression models used are those including the parameters and interactions that have been identified as significant by the stepwise regression procedure (see Table 4 and Table A.3). The optimal combinations of parameters that optimize the response curves are obtained, firstly for optimizing all responses jointly (general scenario), and then a set of responses (scenarios I, II, IIIa and IIIb, IVa and IVb), as summarized in Table 5. Since the joint optimization has to satisfy the requirements for all the selected responses, the more responses to be optimized, the more difficult it is to achieve high predictability due to the conflicting objectives. Therefore, different scenarios are analyzed in order to improve the percentage of predictability of responses.

In the general scenario, all responses are considered and optimized. In detail, the printing time, energy consumption and surface roughness are minimized, while all the dimensions are set to their target values. When different responses are optimized together, for each *j*-th response, an index "d_j" is provided. It represents the individual desirability and evaluates how the settings optimize the response. For instance, if the objective is to minimize the *j*-th response, d_j is calculated as:

$$d_j = 0 \text{ if } \widehat{y}_j > U_j$$
$$d_j = (U_j - \widehat{y}_j)/(U_j - T_j) \text{ if } T_j \leq \widehat{y}_j \leq U_j$$
$$d_j = 1 \text{ if } \widehat{y}_j < T_j$$

where $\widehat{y}_j$ is the predicted value of the *j*-th response, U_j, T_j and L_j are, respectively, the highest acceptable value, the lowest acceptable value and the target value for the *j*-th response.

From the weighted geometric mean of the individual desirabilities, the composite desirability "D", which evaluates how the settings optimize the overall set of responses, is obtained. The optimal solution is achieved when the composite desirability obtains its maximum. In
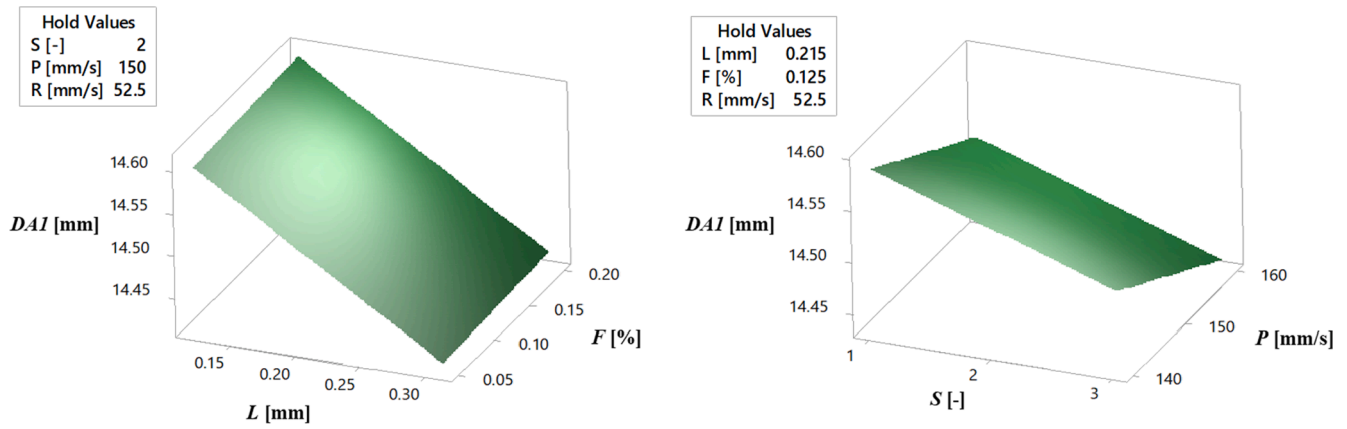
Fig. 8. Surface plots of *DA1* [mm] versus *F* [%] and *L* [mm], and *DA1* [mm] versus *P* [mm/s] and *S* [–]
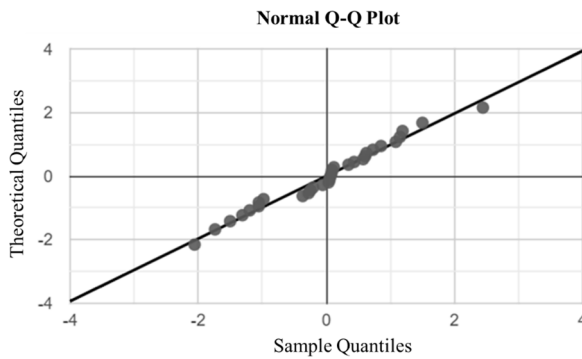

Fig. 9. Normal Q-Q plot of externally studentized residuals for *DA1* [mm]

detail, the formula for the composite desirability, when the importance is the same for each response, is:

$$D = (d_1 \cdot d_2 \cdot d_3 \cdot \cdots \cdot d_n)^{1/n} \tag{3}$$

where *n* is the total number of responses optimized in the scenario and d_j represents the individual desirability for the *j*-th response ($i = 1, …, n$). For instance, if two responses are minimized and the obtained individual desirabilities are $d_1 = 80\%$ and $d_2 = 90\%$, the composite desirability is $D = (d_1 \cdot d_2)^{1/2} = 84.85\%$.

When all the responses are considered, the composite desirability obtained is $D = 70.86\%$ and the configuration of the process parameters is: layer height = 0.26 mm, fill density = 13%, extruder temperature = 215 °C, number of shells = 2, printing speed = 147 mm/s and retraction speed = 54 mm/s. Therefore, all process parameters must be set to an intermediate value in order to optimize all responses together. The

optimal responses with the relevant standard error and prediction intervals are obtained using these process parameters.

In order to optimize each variable at a time, or group of similar variables such as dimensional accuracy and surface roughness, further four scenarios are created. In the I scenario, the printing time is minimized, and the other responses are not optimized. The process parameters which result in the best printing time, which is 52.75 min, are maximum layer height (0.31 mm), minimum fill density (5%) and minimum number of shells (1). The other process parameters, i.e., *T*, *P* and *R*, can be set to any value in their range (minimum value-maximum value, see Table 2) because they are not significant in predicting the printing time. Indeed, as shown in Table 4, their effect on printing time was not statistically significant.

In the II scenario, the goal is to minimize energy consumption, while the other target variables are not optimized. With layer height set to the maximum (0.31 mm), fill density to the minimum (5%), extruder temperature to 220 °C and number of shells to 1, the optimal energy consumption obtained is 2.79 kWh. As for the printing time, *L* is the maximum value, as well as *T*, whereas *F* and *S* are at their minimum value. The values obtained are reasonable and reflect the system's physical nature, except for the temperature that, however, contributes only marginally to the variations of energy consumption.

In the III scenario, the responses of the overhang's surface roughness are first minimized and then those of the bridge. In the first case – III scenario (a) – *Ra1*, *Ra2*, *RSm1* and *RSm2* are optimized (composite desirability $D = 86.83\%$). The optimal process parameters obtained are layer height = 0.12 mm, fill density = 5%, extruder temperature = 220 °C, number of shells = 1, printing speed = 140 mm/s, and retraction speed = 60 mm/s. Therefore, *L*, *S*, *F*, and *P* have to be set at their minimum value, whereas *T* and *R* at their maximum value. In the second case – III scenario (b) -, for the bridge, optimizing *Ra3*, *Ra4*, *Ra5* and *RSm3*, *RSm4*, *RSm5* the optimal process parameters obtained are layer

Table 5
Optimization scenarios.

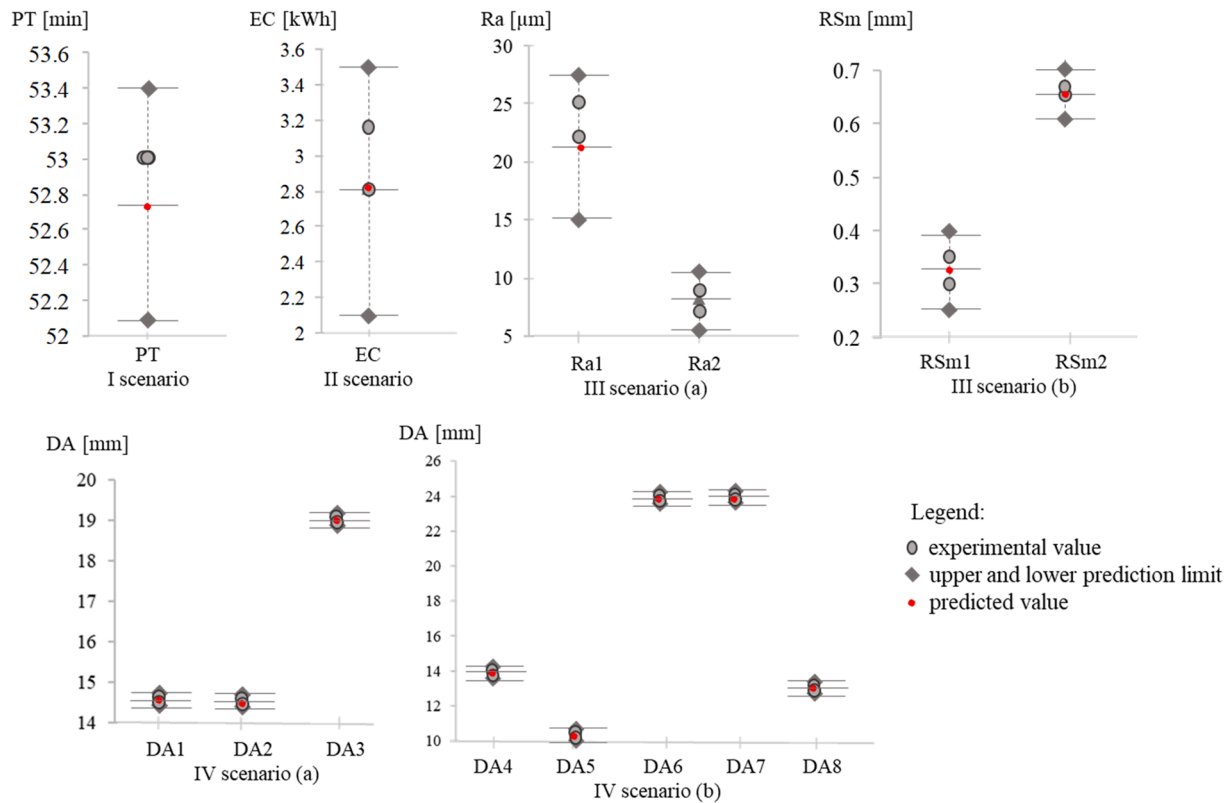|	Responses to be optimized					
	Printing time *PT*	Energy consumption *EC*	Overhang surface roughness *Ra1, Ra2* and *RSm1, RSm2*	Bridge surface roughness *Ra3, Ra4, Ra5* and *RSm3, RSm4, RSm5*	Overhang dimensional accuracy *DA1, DA2, DA3*	Bridge dimensional accuracy *DA4, DA5, DA6, DA7, DA8*
General scenario	X	X	X	X	X	X
I	X					
II		X				
IIIa			X			
IIIb				X		
IVa					X	
IVb						X

Fig. 10. Experimental validation of scenarios I, II, III and IV: experimental values, predicted values and prediction intervals.

height = 0.31 mm, fill density = 20%, extruder temperature = 205 °C, number of shells = 1, printing speed = 160 mm/s and retraction speed = 60 mm/s. In such a case, the composite desirability is 62.19%. Thus, T and S parameters are at the minimum level and L, F, P and R at the maximum level. When comparing the parameters obtained with those of the overhang, it is evident that for T, L, F and P the opposite setting occurs, while parameters S and R may be set at the same value. Hence, while the overhang requires low layer height levels, fill density and printing speed, and high value of temperature, the bridge is characterized by lower surface roughness if built with high layer height, density and printing speed, but with low values of temperature. The underlying reason is the geometric and structural differences between the two samples (see Fig. 4).

In the IV scenario, the aim is to maximize the overhang's dimensional accuracy and that of the bridge. For the first – IV scenario (a) – the process parameters which lead to the target values of the dimensions are layer height = 0.26 mm, fill density = 13%, extruder temperature = 220 °C, number of shells = 2, printing speed = 140 mm/s, and retraction speed = 53 mm/s. In this case, the composite desirability D is 100%. Therefore, to obtain better dimensional accuracy, T should achieve high values and P low values, while L, F, S and R must be set to intermediate values. When optimizing the dimensional accuracy of the bridge – IV scenario (b) – the parameters which should be used are: layer height = 0.27 mm, fill density = 19%, extruder temperature = 211 °C, number of shells = 2, printing speed = 159 mm/s, and retraction speed = 45 mm/s. In such a case, F, P and L assume high values, T and S intermediate values and R low values. In this case, the composite desirability is D = 99.59%. The differences between the process parameters obtained for the overhang and the bridge, mainly referring to the print speed, are

again due to geometric and structural reasons. Consequently, choosing the parameters to be used becomes closely linked to the goal of the optimization.

4.4. Experimental validation

In order to test the adequacy of the models relating each response with the process parameters and, accordingly, the set of parameters that optimize the response(s) in each scenario (see Section 4.3), experimental validations are performed. The method adopted for the validation consists of verifying if the experimental value of each j-th response ($j = 1,…,$ 20) of *ad-hoc* produced samples falls within the corresponding prediction interval. It has to be reminded that each j-th response prediction interval is the range in which the predicted j-th response for a new observation is expected to fall (Montgomery et al., 2012).

Specifically, four new parts are produced for each scenario, and the related responses are measured using the same approach described in Section 3.2. After that, the responses' obtained experimental values are compared with the corresponding predicted values (obtained by exploiting the prediction models) and the prediction intervals, calculated using the software MINITAB®.

In the first scenario, the optimal set of parameters leading to the best printing time is validated by the production of 4 samples. The values of T, P and R are set randomly in the range between 205 °C and 220 °C, 140 mm/s and 160 mm/s, 45 mm/s and 60 mm/s, respectively, because they are not statistically significant in predicting the printing time, while L, F and S are set to their optimal value. As shown in Fig. 10, all the experimental values fall within the printing time's prediction interval, thus demonstrating the adequacy of the prediction model.

In the second scenario, the combination of parameters resulting in the minimum value of energy consumption is validated through the other four samples' production. The parameters used are those obtained from the optimization, except for *P* and *R* that are set at random values in their range.

In the third scenario, which aims at minimizing the roughness of the overhang, III scenario (a), and of the bridge, III scenario (b), two overhang samples and two bridge samples are produced, using the optimal set of parameters reported in Section 4.3.

Finally, in the last scenario, in which the dimensional accuracy is optimized separately for the overhang, IV scenario (a), and for the bridge, IV scenario (b), again two overhang samples and two bridge samples are produced using the optimal set of parameters.

The experimental values and the related prediction intervals of the responses, separately for each scenario, are shown in Fig. 10.

5. Conclusions

This study presents a statistical analysis to investigate the cause-and-effect relationships among selected process parameters and output variables within the MakerBot z18 system. These experimental models are used to improve the FDM process in terms of efficiency and product quality. The macro responses analyzed in the experiments included printing time, energy consumption, surface quality and dimensional accuracy. These were split into twenty responses and measured on the PLA samples produced. By combining literature analysis and practical experience, six process parameters were selected and then analyzed by a two-level factorial with half fractional design. Accordingly, 32 tests were carried out, and the produced samples were examined to study the effect of process parameters and their interactions on the mentioned responses. The six process parameters considered were: layer height, fill density, extruder temperature, number of shells, printing speed and retraction speed. Firstly, through the ANOVA, the significance of every single main effect and interactions between process parameters was derived separately for each response. In addition, a differentiation among the factors with *p*-value $\leq$ 1% (a very significant influence), *p*-value $\leq$ 5% (a significant influence) and *p*-value > 5% (no influence) has been introduced. Then, in order to select only significant factors, the standard stepwise regression was applied. Twenty final regression models were obtained.

Because of the high number of variables and interactions, five different optimization scenarios were analyzed (one general and four specific), and the optimal settings of the parameters were determined for each goal selected. In the general scenario, all responses are jointly optimized. It was found that the process parameters must be set to intermediate values to optimize both part quality and process efficiency. Regarding process efficiency, less dense workpieces with thicker layers and fewer shells ensure minimum process time and energy consumption. To minimize surface roughness, the different geometric and structural characteristics of the parts need to be considered. Specifically, the experimental results have shown that while the overhang requires low values of layer height, fill density and printing speed and a high value of temperature, the bridge needs opposite parameter settings. Finally, to maximize dimensional accuracy, the design features of parts have a key role. For instance, low printing speed is necessary to achieve better dimensional accuracy for overhangs, which leads to opposite results for bridges. Therefore, the evaluation of such experimental results shows that process parameters' optimal settings can vary according to the considered optimization objective. Moreover, optimizing different responses together, especially if they are heterogeneous, may lead to reduce the percentage of their predictability. The insights gained from this study may be of assistance to production designers in the continuous improvement of FDM efficiency and quality of products, both prototypes and finished parts.

Further investigations will be carried out to include star points in the experimental plan, in addition to the central points, to investigate the curvature and estimate the effect of the quadratic terms that were not included in the preliminary models. Moreover, different weights could be assigned to the responses in the optimization scenarios, giving more importance to some objectives and less to others. Future research will be conducted to assess the models' adequacy and the optimal parameters settings by producing different geometries and using different materials or machines. Finally, different modeling approaches (e.g., grey box and white box) could be used to combine the statistical knowledge with the physical relationships.

CRediT authorship contribution statement

Maurizio Galetto: Conceptualization, Methodology, Resources, Writing - review & editing, Supervision, Project administration, Funding acquisition. **Elisa Verna:** Investigation, Data curation, Writing - original draft, Visualization. **Gianfranco Genta:** Software, Validation, Formal analysis.

Appendix A

A.1 Detail on the experiments

This section contains the detail on the measurements of the responses described in Section 3.2. Table A1.

A.2 Detail on data analysis

This section contains further tables related to the data analysis described in Section 4.

Table A2 refers to the *p*-values table obtained from the ANOVA presented in Section 4.1. In the table, the factors which have *p*-values equal or less than 1% are double-asterisked, while *p*-values equal or less than 5% are asterisked.

Table A3 contains the regression models related to the analysis performed using the stepwise regression in Section 4.1 (see also Table 4).

Fig. A1 provides additional normal Q-Q plots and normality test results on externally studentized residuals related to the regression models of Table A.3 for selected responses.

Table A4 refers to the *p*-values table obtained from the ANOVA after the stepwise regression related to the DoE, including four central points, as detailed in Section 4.2. In the table, the factors which have *p*-values equal or less than 1% are double-asterisked, while *p*-values equal or less than 5% are asterisked.

Table A1

Measurement results for the responses of the implemented DoE.

| Run Order	PT [min]	EC [kWh]	DA1 [mm]	DA2 [mm]	DA3 [mm]	DA4 [mm]	DA5 [mm]	DA6 [mm]	DA7 [mm]	DA8 [mm]	Ra1 [μm]	Ra2 [μm]	Ra3 [μm]	Ra4 [μm]	Ra5 [μm]	RSm1 [mm]	RSm2 [mm]	RSm3 [mm]	RSm4 [mm]	RSm5 [mm]
1	58	3.40	14.43	14.40	19.95	14.15	10.16	24.33	24.34	13.54	83.63	25.23	43.70	20.53	26.27	1.038	0.627	0.497	0.582	0.385
2	141	19.67	14.51	14.77	19.44	13.85	10.03	24.01	24.01	13.55	22.27	8.36	81.80	7.33	22.17	0.328	0.637	0.802	0.566	0.365
3	65	4.29	14.51	14.65	19.33	13.78	10.00	24.21	24.24	13.72	36.77	27.47	40.13	13.27	28.33	0.475	0.743	0.509	0.570	0.438
4	65	4.47	14.54	14.62	19.43	13.85	10.03	24.06	24.12	13.54	38.23	21.93	33.90	14.12	24.30	0.512	0.698	0.424	0.570	0.358
5	66	4.81	14.39	14.31	19.83	14.05	10.18	24.29	24.27	13.61	70.73	19.97	46.40	18.40	33.03	0.867	0.571	0.568	0.855	0.469
6	65	3.96	14.22	14.49	19.39	13.77	10.06	24.28	24.29	13.83	35.27	24.53	59.73	10.31	28.17	0.479	0.644	0.657	0.537	0.443
7	66	4.53	14.29	14.19	19.65	13.88	10.16	24.18	24.21	13.71	62.97	21.27	44.47	13.00	32.47	0.765	0.585	0.527	0.678	0.541
8	53	3.09	14.08	14.53	19.08	13.94	10.03	24.27	24.30	13.54	37.73	23.20	38.63	20.83	29.53	0.524	0.590	0.465	0.455	0.417
9	58	3.55	14.03	14.18	19.67	14.07	10.08	24.28	24.25	13.65	61.30	18.23	43.83	19.37	27.73	0.731	0.551	0.481	0.662	0.409
10	65	4.59	14.63	14.43	19.35	13.95	10.17	24.10	24.14	13.33	39.70	26.07	36.67	15.23	26.50	0.503	0.720	0.515	0.674	0.422
11	58	2.93	14.19	14.16	19.73	14.02	10.03	24.37	24.43	13.62	65.13	18.07	44.67	18.87	29.07	0.820	0.511	0.580	0.547	0.467
12	132	16.69	14.36	14.28	19.43	13.85	10.24	24.03	24.09	13.70	22.80	9.19	90.00	9.85	25.33	0.369	0.637	0.851	0.518	0.348
13	53	3.05	14.60	14.41	19.09	13.73	10.03	24.25	24.34	13.58	37.07	23.73	39.03	19.17	38.23	0.480	0.595	0.502	0.462	0.549
14	142	19.07	14.62	14.30	19.45	13.85	10.10	24.17	24.22	13.75	24.23	9.90	78.10	8.79	35.67	0.345	0.681	0.811	0.630	0.528
15	132	16.93	14.56	14.55	19.42	13.88	10.06	24.11	24.20	13.81	24.73	10.71	85.43	8.80	34.17	0.364	0.600	0.719	0.598	0.544
16	142	20.12	14.51	14.56	19.49	13.86	9.89	24.07	24.18	13.84	22.20	11.02	78.57	8.06	29.30	0.326	0.711	0.764	0.647	0.473
17	125	14.97	14.71	14.68	19.09	13.77	10.15	24.10	24.10	13.74	21.73	7.05	88.57	11.42	21.30	0.332	0.574	0.881	0.602	0.347
18	125	14.63	14.70	14.46	19.09	13.86	10.12	24.12	24.19	13.61	22.30	8.10	91.40	8.38	27.00	0.342	0.625	0.873	0.638	0.458
19	141	17.99	14.49	14.61	19.29	13.94	10.00	24.18	24.19	13.88	21.87	10.88	83.57	12.08	27.10	0.354	0.641	0.769	0.608	0.460
20	125	15.24	14.72	14.75	19.33	13.79	10.02	24.16	24.22	13.52	21.27	14.20	80.83	13.77	25.20	0.328	0.714	0.781	0.605	0.425
21	141	18.86	14.50	14.63	19.26	13.89	10.00	24.12	24.09	13.48	15.53	12.03	89.77	11.92	16.83	0.243	0.726	0.846	0.743	0.284
22	142	19.02	14.63	14.53	19.29	13.87	10.51	24.08	24.10	13.67	19.70	17.40	78.67	10.02	22.63	0.292	0.807	0.751	0.629	0.380
23	125	14.35	14.67	14.58	19.14	13.89	10.90	24.25	24.26	13.81	22.27	8.01	90.33	12.69	17.87	0.353	0.653	0.824	0.622	0.274
24	66	4.43	14.52	14.32	19.61	14.00	10.30	24.28	24.32	13.62	56.23	16.80	62.90	14.57	23.67	0.698	0.587	0.654	0.530	0.334
25	53	3.01	14.67	14.57	19.00	13.75	10.17	24.13	24.13	13.97	41.53	21.57	61.00	24.53	23.07	0.516	0.550	0.726	0.412	0.330
26	141	18.11	14.66	14.81	19.26	13.85	10.40	24.04	24.01	13.86	22.30	9.49	79.63	20.23	14.87	0.297	0.657	0.736	0.372	0.247
27	132	17.53	14.81	14.53	19.30	13.81	10.12	24.11	24.07	13.77	15.10	10.84	77.10	14.43	15.57	0.253	0.701	0.749	0.442	0.233
28	132	17.35	14.49	14.38	19.27	13.79	10.20	24.12	24.09	13.74	15.57	8.60	78.47	11.16	15.80	0.245	0.779	0.720	0.496	0.248
29	58	3.61	14.48	14.40	19.55	13.97	10.21	24.31	24.31	13.76	49.60	16.93	57.13	19.97	22.80	0.633	0.548	0.715	0.451	0.321
30	66	4.42	14.50	14.43	19.57	13.92	10.24	24.27	24.25	13.74	66.53	15.03	61.83	16.77	26.10	0.779	0.591	0.648	0.428	0.397
31	53	2.83	14.64	14.71	19.22	13.80	10.12	24.39	24.39	13.85	41.60	20.03	57.30	22.50	25.87	0.514	0.592	0.634	0.425	0.402
32	142	19.87	14.74	14.69	19.31	13.87	10.14	24.08	24.08	14.02	18.77	7.66	85.70	13.67	20.97	0.287	0.658	0.876	0.452	0.305

Table A2
p-value [%] table resulting from the ANOVA.

|	PT [min]	EC [kWh]	DA1 [mm]	DA2 [mm]	DA3 [mm]	DA4 [mm]	DA5 [mm]	DA6 [mm]	DA7 [mm]	DA8 [mm]	Ra1 [μm]	Ra2 [μm]	Ra3 [μm]	Ra4 [μm]	Ra5 [μm]	RSm1 [mm]	RSm2 [mm]	RSm3 [mm]	RSm4 [mm]	RSm5 [mm]
L [mm]	<0.1**	<0.1**	0.3**	<0.1**	<0.1**	2.8*	29.1	<0.1**	<0.1**	20.6	<0.1**	<0.1**	<0.1**	<0.1**	2.2*	<0.1**	1.1*	<0.1**	54.4	13.3
F [%]	<0.1**	<0.1**	87.6	12.0	2.1*	78.6	61.1	1.0**	2.4*	94.5	73.9	42.6	65.2	2.0*	79.3	39.0	4.3*	79.0	9.5	55.3
T [°C]	100	0.3**	87.6	30.5	88.0	67.6	5.3*	2.0*	3.2*	32.1	19.8	76.4	28.7	60.5	16.0	21.8	90.7	96.7	48.6	23.3
S [–]	<0.1**	<0.1**	11.3	<0.1**	<0.1**	0.5**	64.3	18.3	32.1	40.1	<0.1**	15.6	93.4	52.7	39.1	<0.1**	55.6	95.2	60.3	73.0
P [mm/s]	100	60.7	16.5	88.0	30.3	94.1	33.3	70.9	89.6	92.6	17.0	75.9	76.4	39.3	52.2	15.3	73.4	51.5	76.9	41.1
R [mm/s]	100	56.0	1.2*	48.4	90.6	74.9	11.5	66.0	73.5	83.5	47.0	39.8	91.1	40.3	20.4	51.4	83.4	51.1	58.9	31.7
L·F [mm]	<0.1**	<0.1**	28.7	20.8	80.1	17.9	22.7	18.3	42.6	38.9	68.5	84.2	63.3	1.5*	79.3	84.1	35.8	91.8	20.2	93.0
L·T [mm·°C]	100	1.8**	53.5	2.0*	58.2	19.4	5.5	22.6	81.4	98.2	62.1	92.5	60.6	67.6	23.9	34.9	33.1	78.3	35.7	28.6
L·S [mm]	0.3**	<0.1**	29.8	25.3	0.1**	0.3**	20.4	1.6*	23.7	28.2	<0.1**	4.6*	21.8	42.8	29.4	<0.1**	2.7*	35.1	9.5	62.3
L·P [mm²/s]	100	92.4	21.1	1.7*	16.5	45.1	32.2	25.0	37.0	50.7	16.6	60.9	99.5	63.6	52.3	10.0	52.1	72.3	81.6	62.9
L·R [mm²/s]	100	45.8	17.2	32.4	80.1	64.1	2.7*	7.5	8.6	96.3	30.0	73.7	92.4	46.9	29.8	42.7	42.3	76.0	66.9	21.8
F·T [°C]	100	12.9	79.5	43.4	6.0	15.3	78.4	18.3	77.4	22.1	8.8	98.4	56.6	33.0	17.8	7.2	71.6	40.7	2.6*	25.0
F·S [–]	<0.1**	0.9**	6.1	78.0	1.0**	16.6	15.1	16.5	9.4	36.5	57.5	49.9	31.5	61.7	11.4	75.1	35.7	19.9	80.3	19.0
F·P [mm/s]	100	53.8	41.2	91.4	85.3	74.9	99.0	44.1	29.8	42.6	15.6	96.2	27.9	73.3	52.6	12.1	40.6	14.8	33.8	94.5
F·R [mm/s]	100	33.7	11.3	10.4	65.2	22.6	71.2	3.3*	37.0	100	79.5	31.1	98.1	59.8	91.9	78.7	84.9	85.0	30.5	72.7
T·S [°C]	100	49.9	62.2	94.9	47.6	22.6	74.8	2.6*	10.3	3.5*	22.9	60.7	97.2	64.7	88.4	23.4	83.3	77.6	46.2	91.0
T·P [°C·mm/s]	100	49.2	64.1	62.3	58.2	78.6	95.2	61.2	77.4	41.3	96.8	94.1	78.4	90.6	66.6	97.5	48.4	88.2	19.9	62.9
T·R [°C·mm/s]	100	82.1	23.7	28.7	47.6	78.6	1.5**	70.9	32.1	53.6	12.5	90.4	15.5	5.2	1.8*	6.9	72.1	12.2	78.3	1.6*
S·P [mm/s]	100	81.5	25.6	4.3*	2.8*	13.1	69.4	8.4	3.5*	13.3	22.2	41.5	43.1	43.8	10.4	4.6*	86.3	60.8	31.7	23.9
S·R [mm/s]	100	70.1	35.8	0.4**	36.6	64.1	24.4	20.4	97.9	22.9	29.1	21.5	70.6	34.1	48.5	23.0	21.8	76.8	14.5	28.3
P·R [mm²/s²]	100	67.6	11.3	7.3	96.0	71.2	35.6	61.2	42.6	59.7	57.3	21.2	69.5	44.1	65.0	55.0	24.5	64.7	7.9	68.4
R-Sq [%]	99.99	99.92	84.14	93.27	93.40	83.77	80.21	92.49	88.04	68.09	97.57	90.79	92.07	85.90	77.83	97.53	75.85	85.81	75.31	71.70
R-Sq adj [%]	99.96	99.75	50.84	79.13	79.55	49.69	38.64	76.73	62.93	1.09	92.48	71.43	75.41	56.29	31.27	92.35	25.14	56.00	23.47	12.27

Table A3

Regression models obtained after stepwise regression.

| Response	Regression equation
PT [min]	$PT = 161.757 - 378.03L + 135.23F + 3.796S - 118.0L \cdot F + 0.31L \cdot S - 16.13F \cdot S$
EC [kWh]	$EC = 6.01 - 4.0L - 5.5F + 0.0635T + 1.545S - 65.84L \cdot F - 0.2501L \cdot T - 3.409L \cdot S + 0.1867F \cdot T - 2.710F \cdot S$
DA1 [mm]	$DA1 = 11.02 + 1.56L - 0.0995S + 0.0249P + 0.0839R - 0.0482L \cdot R + 0.471F \cdot S - 0.0152F \cdot R - 0.000542P \cdot R$
DA2 [mm]	$DA2 = 14.494 + 5.97L - 1.75L - 0.273S - 2.68L \cdot F - 0.00101L \cdot T - 0.0412L \cdot P + 0.0504F \cdot R + 0.00339S \cdot P - 0.00655S \cdot R + 0.000035P \cdot R$
DA3 [mm]	$DA3 = 19.002 - 1.34L - 1.19F + 0.357S + 0.859L \cdot S + 0.0031L \cdot P + 0.0159F \cdot T - 0.763F \cdot S - 0.00199S \cdot P$
DA4 [mm]	$DA4 = 13.8003 - 4.15L + 0.598S - 2.62L \cdot F + 0.0178L \cdot T + 0.510L \cdot S + 0.00827F \cdot T - 0.256F \cdot S - 0.01198F \cdot R - 0.00265T \cdot S - 0.000444S \cdot P$
DA5 [mm]	$DA5 = -3.43 + 0.0572T + 0.3108R + 0.18L \cdot F + 0.02364L \cdot T + 0.114L \cdot S - 0.1059L \cdot R - 0.023F \cdot S - 0.001328T \cdot R$
DA6 [mm]	$DA6 = 24.901 - 0.942L + 1.821F - 0.00353T + 0.254L \cdot S + 0.02236L \cdot R - 0.0419F \cdot R + 0.000121T \cdot S - 0.000445S \cdot P$
DA7 [mm]	$DA7 = 25.127 + 0.577L - 0.959F - 0.00466T + 0.00298L \cdot R + 0.273F \cdot S + 0.000391T \cdot S - 0.000697S \cdot P$
DA8 [mm]	$DA8 = 13.7397 - 0.375L - 0.00029F \cdot T - 0.000140T \cdot S + 0.00060S \cdot P - 0.00070S \cdot R$
Ra1 [µm]	$Ra1 = -73.8 + 237L + 0.213T + 42.4S + 0.351P + 70.6L \cdot S - 1.45L \cdot P - 0.373F \cdot T + 0.51F \cdot P - 0.157T \cdot S - 0.000398T \cdot R - 0.1198S \cdot P$
Ra2 [µm]	$Ra2 = 3.59 + 87.2L + 0.68S - 14.54L \cdot S + 0.0289S \cdot R - 0.000601P \cdot R$
Ra3 [µm]	$Ra3 = 162.0 - 192.8L - 0.248T + 3.20L \cdot S + 2.6F \cdot S - 0.098F \cdot P - 0.000183T \cdot R$
Ra4 [µm]	$Ra4 = 6.91 + 60.9L + 28.6F - 226.8L \cdot F - 0.000266T \cdot R$
Ra5 [µm]	$Ra5 = 123.1 - 292L - 0.437T + 1.49L \cdot T - 0.154F \cdot T + 18.1F \cdot S - 0.000667T \cdot R - 0.0100S \cdot P$
RSm1 [mm]	$RSm1 = -0.513 + 3.05L + 0.245S + 0.00593P + 0.797L \cdot S - 0.0194L \cdot P - 0.00787F \cdot T + 0.0104F \cdot P - 0.000005T \cdot R - 0.00231S \cdot P$
RSm2 [mm]	$RSm2 = 0.6546 + 0.209L + 0.338F - 0.2849L \cdot S + 0.001029S \cdot R - 0.000011P \cdot R$
RSm3 [mm]	$RSm3 = 1.026 - 1.201L + 0.0678F \cdot S - 0.00123F \cdot P - 0.000007T \cdot R$
RSm4 [mm]	$RSm4 = 0.691 - 6.85F + 0.14L \cdot F + 0.005L \cdot S + 0.0340F \cdot T - 0.000005T \cdot P + 0.000182S \cdot R - 0.000005P \cdot R$
RSm5 [mm]	$RSm5 = 0.714 - 1.095L + 0.0256L \cdot R + 0.0807F \cdot S - 0.000035T \cdot R$
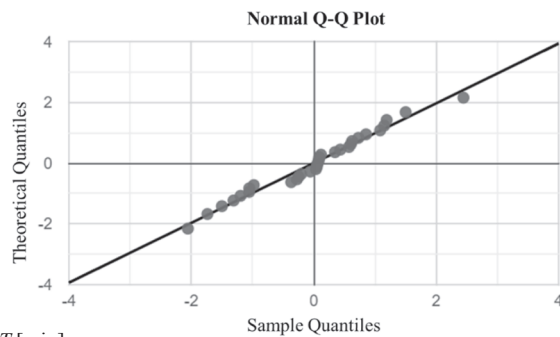
PT [min]
Skewness test: p-value=0.95, Kurtosis test: p-value=0.53, Shapiro-Wilk test: p-value= 0.59. No outliers detected.
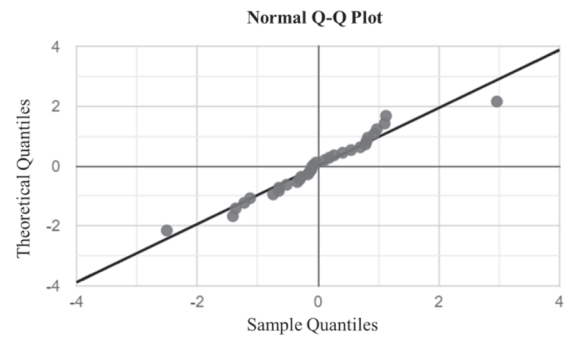
EC [kWh]
Skewness test: p-value=0.53, Kurtosis test: p-value=0.06, Shapiro-Wilk test: p-value= 0.39. 1 outlier detected (test no. 2).
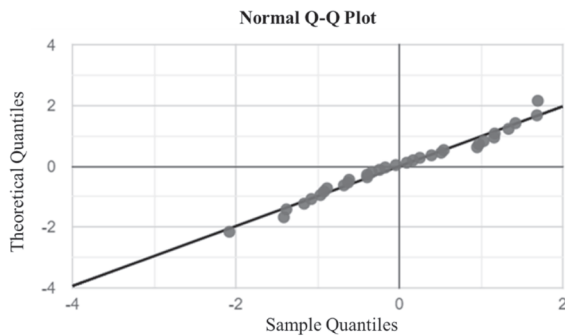
Ra5 [µm]
Skewness test: p-value=0.95, Kurtosis test: p-value=0.17, Shapiro-Wilk test: p-value= 0.41. No outliers detected.
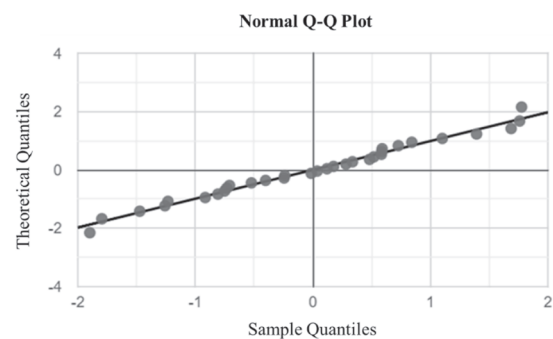
RSm5 [mm]
Skewness test: p-value=0.96, Kurtosis test: p-value=0.44, Shapiro-Wilk test: p-value= 0.53. No outliers detected.

Fig. A1. Normal Q-Q plots and normality tests results ($\alpha = 0.05$) on externally studentized residuals for the responses PT, EC, Ra5 and RSm5.

Table A4

p-value [%] table resulting from ANOVA after the stepwise regression (Alpha-to-Enter = Alpha-to-Remove = 15%) including four central points. Quadratic effect means $L{\cdot}L$ alias $F{\cdot}F$ alias $T{\cdot}T$ alias $S{\cdot}S$ alias $P{\cdot}P$ alias $R{\cdot}R$.

	PT [min]	EC [kWh]	DA1 [mm]	DA2 [mm]	DA3 [mm]	DA4 [mm]	DA5 [mm]	DA6 [mm]	DA7 [mm]	DA8 [mm]	Ra1 [µm]	Ra2 [µm]	Ra3 [µm]	Ra4 [µm]	Ra5 [µm]	RSm1 [mm]	RSm2 [mm]	RSm3 [mm]	RSm4 [mm]	RSm5 [mm]
L [mm]	<0.1**	<0.1**	<0.1**	0.4**	<0.1**	0.1**		<0.1**	<0.1**	8.9	<0.1**	<0.1**	<0.1**	<0.1**	0.7**	<0.1**	<0.1**	<0.1**		8.8
F [%]	<0.1**	<0.1**			0.2**			0.8**	1.1*					0.1**			0.6**		3.0*	
T [°C]		<0.1**					1.1*	1.9*	1.6*		9.5		9.6		11.7	11.3				
S [–]	<0.1**	<0.1**	4.7*	<0.1**	<0.1**	<0.1**					<0.1**	5.1				<0.1**				
P [mm/s]			8.3								7.5					6.5				
R [mm/s]			0.1**				4.1													
Quadratic effect	<0.1**	<0.1**			<0.1**						<0.1**			<0.1**		<0.1**				
L·F [mm]	<0.1**	<0.1**				4.8*	12.1							0.1**					10.3	
L·T [mm·°C]		0.1**		10.1		5.6	1.2*													
L·S [mm]	<0.1**	<0.1**			<0.1**	<0.1**	10.2	1.4*		15.0	<0.1**	0.6**	5.4			<0.1**	0.2**		3.1*	
L·P [mm²/s]			12.0	9.1	6.4							7.2				3.3*				
L·R [mm²/s]			8.9				0.3**	8.3	6.0											14.0
F·T [°C]		3.8*			1.1*	3.5				10.1		2.6*			13.5	1.9*			0.3**	
F·S [–]	<0.1**	<0.1**	1.7*		<0.1**	4.1	6.3		6.7				11.7		7.6				5.4	
F·P [mm/s]											6.5		9.0			4.5*		2.9*		
F·R [mm/s]			4.7			7.4		3.3*												
T·S [°C]						7.4		2.5*	7.4	0.4**	11.9					12.6				
T·P [°C·mm/s]																			10.0	
T·R [°C·mm/s]			14.3				0.1**				4.5		2.6*	0.8**	0.5**	1.8*		2.0*		0.4**
S·P [mm/s]					0.3**	2.6*		9.3	1.8*	4.2	11.3				6.7	0.9**				
S·R [mm/s]				3.0*			13.5			10.7			9.0			12.3	10.1		6.1	
P·R [mm²/s²]			4.7*									8.7					12.3		2.3*	
R-Sq [%]	99.97	99.89	72.94	61.79	89.41	80.53	67.77	76.72	71.25	46.85	96.68	84.57	90.18	76.92	50.31	96.73	58.05	79.57	53.35	31.90
R-Sq adj [%]	99.96	99.84	62.11	52.88	86.27	72.75	56.62	69.82	64.06	35.85	94.95	82.00	88.14	73.07	40.03	94.79	51.06	76.93	45.44	25.52

Appendix B. Supplementary material

Supplementary data to this article can be found online at https://doi.org/10.1016/j.cie.2021.107238.

References

Abid, S., Messadi, R., Hassine, T., Daly, H. Ben, Soulestin, J., & Lacrampe, M. F. (2018). Optimization of mechanical properties of printed acrylonitrile butadiene styrene using RSM design. *The International Journal of Advanced Manufacturing Technology*, 1–10.

Agresti, A. (2003). *Categorical data analysis* (Vol. 482). John Wiley & Sons.

Ahn, D., Kweon, J.-H., Kwon, S., Song, J., & Lee, S. (2009). Representation of surface roughness in fused deposition modeling. *Journal of Materials Processing Technology, 209*(15–16), 5593–5600.

Amini, M., & Chang, S. I. (2018). MLCPM: A process monitoring framework for 3D metal printing in industrial scale. *Computers & Industrial Engineering, 124*, 322–330.

Anitha, R., Arunachalam, S., & Radhakrishnan, P. (2001). Critical parameters influencing the quality of prototypes in fused deposition modelling. *Journal of Materials Processing Technology, 118*(1–3), 385–388.

Chergui, A., Hadj-Hamou, K., & Vignat, F. (2018). Production scheduling and nesting in additive manufacturing. *Computers & Industrial Engineering, 126*, 292–301.

Devore, J. L. (2011). *Probability and Statistics for Engineering and the Sciences*. Cengage learning.

Dong, G., Wijaya, G., Tang, Y., & Zhao, Y. F. (2018). Optimizing process parameters of fused deposition modeling by Taguchi method for the fabrication of lattice structures. *Additive Manufacturing, 19*, 62–72.

Durgun, I., & Ertan, R. (2014). Experimental investigation of FDM process for improvement of mechanical properties and production cost. *Rapid Prototyping Journal, 20*(3), 228–235.

Franceschini, F., Galetto, M., & Maisano, D. (2007). *Management by measurement: Designing key indicators and performance measurement systems*. Springer Science & Business Media.

Franceschini, F., Galetto, M., & Maisano, D. (2019). *Designing performance measurement systems. Management for Professionals*. Springer Nature.

Frank, D., Chandra, R. L., & Schmitt, R. (2015). An Investigation of cause-and-effect relationships within a 3D-printing system and the applicability of optimum printing parameters from experimental models to different printing jobs. *3D Printing and Additive Manufacturing, 2*(3), 131–139.

Galetto, M., Genta, G., Maculotti, G., & Verna, E. (2020). Defect probability estimation for hardness-optimised parts by selective laser melting. *International Journal of Precision Engineering and Manufacturing, 21*(9), 1739–1753. https://doi.org/10.1007/s12541-020-00381-1

Gardan, J. (2016). Additive manufacturing technologies: State of the art and trends. *International Journal of Production Research, 54*(10), 3118–3132.

Garg, A., Bhattacharya, A., & Batish, A. (2016). On surface finish and dimensional accuracy of FDM parts after cold vapor treatment. *Materials and Manufacturing Processes, 31*(4), 522–529.

Gibson, I., Rosen, D. W., & Stucker, B. (2014). Additive manufacturing technologies. 2010. Springer.

Griffiths, C. A., Howarth, J., Rowbotham, G.de. A., & Rees, A. (2016). Effect of build parameters on processing efficiency and material performance in fused deposition modelling. *Procedia CIRP, 49*, 28–32.

ISO 16610-31:2016. Geometrical product specifications (GPS) - Filtration - Part 31: Robust profile filters: Gaussian regression filters. International Organization for Standardization.

ISO 4287:2009. Geometrical Product Specifications (GPS) - Surface texture: Profile method - Terms, definitions and surface texture parameters. International Organization for Standardization.

ISO 4288:2000. Geometrical product specifications (GPS) - Surface texture: Profile method - Rules and procedures for the assessment of surface texture. International Organization for Standardization.

Joanes, D. N., & Gill, C. A. (1998). Comparing measures of sample skewness and kurtosis. *Journal of the Royal Statistical Society: Series D (The Statistician), 47*(1), 183–189.

Kaveh, M., Badrossamay, M., Foroozmehr, E., & Etefagh, A. H. (2015). Optimization of the printing parameters affecting dimensional accuracy and internal cavity for HIPS material used in fused deposition modeling processes. *Journal of Materials Processing Technology, 226*, 280–286.

Lan, H., & Ding, Y. (2007). Price quotation methodology for stereolithography parts based on STL model. *Computers & Industrial Engineering, 52*(2), 241–256.

Li, H., Wang, T., Sun, J., & Yu, Z. (2018). The effect of process parameters in fused deposition modelling on bonding degree and mechanical properties. *Rapid Prototyping Journal, 24*(1), 80–92.

Liu, Z., Wang, Y., Wu, B., Cui, C., Guo, Y., & Yan, C. (2019). A critical review of fused deposition modeling 3D printing technology in manufacturing polylactic acid parts. *The International Journal of Advanced Manufacturing Technology*, 1–13.

Lužanin, O., Movrin, D., & Plančak, M. (2014). Effect of layer thickness, deposition angle, and infill on maximum flexural force in FDM-built specimens. *Journal for Technology of Plasticity, 39*(1), 49–58.

Majeed, A., Zhang, Y., Lv, J., Peng, T., Atta, Z., & Ahmed, A. (2020). Investigation of T4 and T6 heat treatment influences on relative density and porosity of AlSi10Mg alloy components manufactured by SLM. *Computers & Industrial Engineering, 139*, Article 106194.

Mason, R. L., Gunst, R. F., & Hess, J. L. (2003). *Statistical design and analysis of experiments: with applications to engineering and science* (Vol. 474). John Wiley & Sons.

Montero, M., Roundy, S., Odell, D., Ahn, S.-H., & Wright, P. K. (2001). Material characterization of fused deposition modeling (FDM) ABS by designed experiments. *Society of Manufacturing Engineers, 10*(13552540210441166).

Montgomery, D. C. (2017). *Design and analysis of experiments* (9th ed.). John Wiley & Sons.

Montgomery, D. C., Peck, E. A., & Vining, G. G. (2012). *Introduction to linear regression analysis* (Vol. 821). John Wiley & Sons.

Montgomery, D. C., Runger, G. C., & Hubele, N. F. (2009). Engineering statistics. John Wiley & Sons.

Myers, R. H., & Montgomery, D. C. (1995). *Response surface methodology: process and product optimization using designed experiments* (Vol. 4). John Wiley & Sons.

Nancharaiah, T., Raju, D. R., & Raju, V. R. (2010). An experimental investigation on surface quality and dimensional accuracy of FDM components. *International Journal on Emerging Technologies, 1*(2), 106–111.

Nyaluke, A. P., An, D., Leep, H. R., & Parsaei, H. R. (1995). Rapid prototyping: Applications in academic institutions and industry. *Computers & Industrial Engineering, 29*(1–4), 345–349.

Onwubolu, G. C. & Rayegani, F. (2014). Characterization and optimization of mechanical properties of ABS parts manufactured by the fused deposition modelling process. International Journal of Manufacturing Engineering 2014.

Pandey, P. M., Reddy, N. V., & Dhande, S. G. (2003). Improvement of surface finish by staircase machining in fused deposition modeling. *Journal of Materials Processing Technology, 132*(1–3), 323–331.

Pandey, P. M., Thrimurthulu, K., & Reddy*, N. V. (2004). Optimal part deposition orientation in FDM by using a multicriteria genetic algorithm. *International Journal of Production Research, 42*(19), 4069–4089.

Pennington, R. C., Hoekstra, N. L., & Newcomer, J. L. (2005). Significant factors in the dimensional accuracy of fused deposition modelling. *Proceedings of the Institution of Mechanical Engineers, Part E: Journal of Process Mechanical Engineering, 219*(1), 89–92.

Perez, C. J. L. (2002). Analysis of the surface roughness and dimensional accuracy capability of fused deposition modelling processes. *International Journal of Production Research, 40*(12), 2865–2881.

Rayegani, F., & Onwubolu, G. C. (2014). Fused deposition modelling (FDM) process parameter prediction and optimization using group method for data handling (GMDH) and differential evolution (DE). *The International Journal of Advanced Manufacturing Technology, 73*(1–4), 509–519.

Sahu, R. K., Mahapatra, S. S., & Sood, A. K. (2013). A study on dimensional accuracy of fused deposition modeling (FDM) processed parts using fuzzy logic. *Journal for Manufacturing Science & Production, 13*(3), 183–197.

Sanatgar, R. H., Campagne, C., & Nierstrasz, V. (2017). Investigation of the adhesion properties of direct 3D printing of polymers and nanocomposites on textiles: Effect of FDM printing process parameters. *Applied Surface Science, 403*, 551–563.

Shapiro, S. S., & Wilk, M. B. (1965). An analysis of variance test for normality (complete samples). *Biometrika, 52*(3/4), 591–611.

Sood, Anoop K, Ohdar, R. K., & Mahapatra, S. S. (2012). Experimental investigation and empirical modelling of FDM process for compressive strength improvement. *Journal of Advanced Research, 3*(1), 81–90.

Sood, Anoop Kumar, Ohdar, R. K., & Mahapatra, S. S. (2009). Improving dimensional accuracy of fused deposition modelling processed part using grey Taguchi method. *Materials & Design, 30*(10), 4243–4252.

Stoof, D., & Pickering, K. (2018). Sustainable composite fused deposition modelling filament using recycled pre-consumer polypropylene. *Composites Part B: Engineering, 135*, 110–118.

Verna, E., Biagi, R., Kazasidis, M., Galetto, M., Bemporad, E., & Lupoi, R. (2020). Modeling of erosion response of cold-sprayed In718-Ni composite coating using full factorial design. *Coatings, 10*(4). https://doi.org/10.3390/coatings10040335

Verna, E., Genta, G., Galetto, M., & Franceschini, F. (2019). Designing offline inspection strategies for Selective Laser Melting Additive Manufacturing processes. *Proceedings of the XIV Convegno Dell'Associazione Italiana Tecnologie Manifatturiere*.

Verna, E., Genta, G., Galetto, M., & Franceschini, F. (2020). Planning offline inspection strategies in low-volume manufacturing processes. *Quality Engineering, 32*(4), 705–720.

Wickramasinghe, S., Do, T., & Tran, P. (2020). FDM-based 3D printing of polymer and associated composite: A review on mechanical properties, defects and treatments. *Polymers, 12*(7), 1529.

Wiegand, R. E. (2010). Performance of using multiple stepwise algorithms for variable selection. *Statistics in Medicine, 29*(15), 1647–1659.

Wohlers, T. (2018). *Wohlers Report 2018: 3D Printing and Additive Manufacturing State of the Industry: Annual Worldwide Progress Report*. Wohlers Associates.

Wu, D., Wei, Y., & Terpenny, J. (2018). Predictive modelling of surface roughness in fused deposition modelling using data fusion. *International Journal of Production Research*, 1–15.